Steady-State Electrical Characteristics of DC Plasma Glow Discharges Used for Thin Film Deposition

Mohammad K. KALAF

Ministry of Science and Technology, Baghdad, IRAQ

Abstract

In this work, the current-voltage characteristics of dc plasma discharges were studied. The current-voltage characteristics of argon gas discharge at different inter-electrode distances and working pressure of 0.7mbar without magnetrons were introduced. Then the variation of discharge current with inter-electrode distance at certain discharge voltages without using magnetron was determined. The current-voltage characteristics of discharge plasma at inter-electrode distance of 4cm without magnetron, with only one magnetron and with dual magnetrons were also determined. The variation of discharge current with inter-electrode distance at certain discharge voltage (400V) for the cases without magnetron, using one magnetron and dual magnetrons were studied. Finally, the discharge current-voltage characteristics for different argon/nitrogen mixtures at total gas pressure of 0.7mbar and inter-electrode distance of 4cm were presented.

1. Introduction

Glow discharge is low-temperature neutral plasma where the number of electrons is equal to the number of ions despite that local but negligible imbalances may exist at walls [1]. Glow discharge is described as self-sustaining plasma, i.e., the avalanche effect of electrons keeps the continuous production of ion species. The avalanche condition from the initial applied voltage in a typical low-pressure discharge is shown in figure (1).

If an initial voltage is applied on a gas sample between two electrodes at sufficient separation, little current will flow through this sample due to the ionization effects in the gas. As the applied voltage is increased to reach the breakdown voltage, the energy given to ions is increased too that increases their collisions with atoms and electrodes [2]. Accordingly, more ions and electrons are produced due to the ionization and secondary electron emission effects, which lead to increase the flowing current gradually approaching the breakdown point beyond which the avalanche occurs and the current increases drastically in the Townsend discharge region [3].
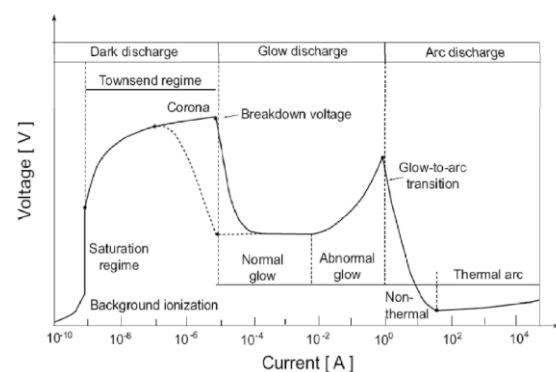

Figure (1) Different regions of plasma discharge on the I-V characteristics [10]

The breakdown voltage is directly related to the pressure of the gas sample and the mean free path of secondary electrons. This relation between breakdown voltage (V_B) and gas pressure (p) is known as "Paschen's law" and given by [4]

$$V_B = \frac{pdB}{\log(pdA) - \log\left(\log\left(1 + \frac{1}{\gamma e}\right)\right)} \qquad (1)$$

where A and B are constants and their values are determined by the properties of the used gas, as shown in Table (1), d is the distance between

discharge electrodes and γ_e is the emission coefficient of the secondary electrons

The breakdown voltage (V_B) depends on the product ($p.d$), and weakly depends on the cathode material that defines the emission coefficient of secondary electrons. As well, the breakdown voltage is proportional to the product $p.d$ at large values of this product and the electric field ($E=V/d$) is scaled linearly with the pressure [5].

In case of small values of the product $p.d$, only few collisions occur and higher voltage is applied to increase the probability of breakdown per collision. Hence, the minimum voltage required to ignite the discharge of a gas sample of pressure p over a distance d is defined at the minimum of Paschen's curve, as [6]

$$pd|_{V_{min}} = \frac{1}{A} \log \left(1 + \frac{1}{\gamma_e}\right) \qquad (2)$$

If the pressure and/or separation distance is too large, ions generated in the gas are slowed by inelastic collisions, so that they strike the cathode with insufficient energy to produce secondary electrons. In most sputtering glow discharges, the discharge starting voltage is relatively high [7]. Figure (2) shows the Paschen's curves of different gases. The electron mean free path (λ_e) is then related to the pressure by

$$\lambda_e \cong p.d \qquad (3)$$

To initiate the discharge, the following condition must be satisfied [8]

$$p \geq \frac{\lambda_e}{d}$$

According to the self-sustaining feature of glow discharge, the number of the produced electrons is just sufficient to produce the same number of ions to generate again the same number of electrons. These ions liberate electrons from the electrodes (secondary), atom-ion and ion-ion collisions [9]. When this condition is satisfied, the voltage decreases and the current increases. This is said to be a "normal discharge".

Due to the recombination effects and excited atoms returning to ground state, the plasma begins to glow, as [10]

$$A^* \rightarrow A + h\nu \qquad (4a)$$
$$A^+ + e^- \rightarrow A + h\nu \qquad (4b)$$
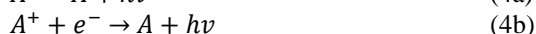
here A^* is an excited atom and e^- is a high-energy electron

Table (2) shows the values of secondary electron emission coefficients for three different metals when different ions are bombarding these targets.
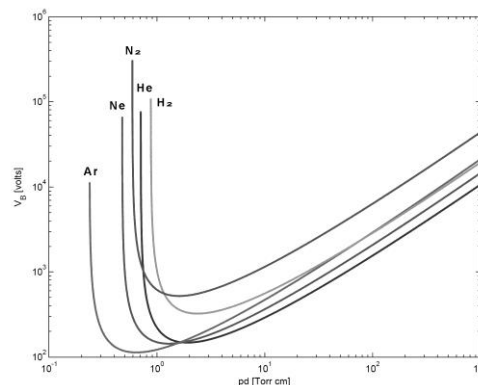

Figure (2) Paschen's curves of different common gases used in electric discharge applications [11]

Table (1) Typical values of A and B constants, E/p and ionization energy (V_i) for various gases [8]

Gas	A	B	E/p	V_i (V)
H_2	5	130	150~600	15.4
N_2	12	342	100~600	15.5
O_2	-	-	-	12.2
CO_2	20	466	500~1000	13.7
air	15	365	100~800	-
H_2O	13	290	150~1000	12.6
HCl	25	380	200~1000	-
He	3	34 (25)	20~150 (3~10)	24.5
Ne	4	100	100~400	21.5
Ar	14	180	100~600	15.7
Kr	17	240	100~1000	14
Xe	26	350	200~800	12.1
Hg	20	370	200~600	10.4

A in (Ion/pairs)/(cm.torr), B in V/(cm.torr), E/p in V/(cm.torr)

Table (2) The secondary electron emission coefficients for three different metals when different ions are bombarding these targets [8]

Target Material	Incident Ion	Ion Energy (eV)		
		200	600	1000
W	He$^+$	0.524	0.24	0.258
	Ne$^+$	0.258	0.25	0.25
	Ar$^+$	0.1	0.104	0.108
	Kr$^+$	0.05	0.054	0.108
	Xe$^+$	0.016	0.016	0.016
Mo	He$^+$	0.215	0.225	0.245
	He^{++}	0.715	0.77	0.78
Ni	He$^+$		0.6	0.84
	Ne$^+$			0.53
	Ar$^+$		0.09	0.156

2. Experimental Part

The magnetron sputtering system used in this work was designed to include vacuum chamber, discharge electrodes and magnetron assembly, vacuum unit, dc power supplies, gas supply system, cooling system and measuring instruments.

The vacuum chamber was constructed from stainless steel. It is a cylinder with internal diameter of 35cm, outer diameter of 45cm, and height of 37.5cm. There were four side holes of 10.8cm in diameter on the circumference of the cylinder; one of them was closed with a quartz window, while the

other three were closed with glass windows. These windows were mounted by stainless steel flanges each of 21cm in diameter and four screws. They were used for monitoring the discharge and events inside the chamber. Each window was far from the discharge region by a neck of 7.5cm diameter to avoid the effects of heat developed by the glow discharge.

The vacuum chamber was sealed from lower end with a stainless steel flange of 40cm in diameter containing a feedthrough for electrical connections required for experiment. The upper end was sealed with a similar flange but containing two feedthroughs; one for gas inlet and Pirani gauge and the other for the Penning gauge. Both flanges include a central hole for the electrode hollow holder. Rubber O-rings and silicon vacuum grease were used in all sealing points.

Both discharge electrodes were constructed from stainless steel (St. St. 304) hollow disks of 80mm in diameter and 8.5mm in thickness. The electrode was joined to holder of 295mm in length and outer and inner diameters of 16.2mm and 11.6mm, respectively, to include a stainless steel channel of 78.5mm in length and 5.6mm in diameter through which the cooling water was flowed to the inside volume of the electrode. The holder tube includes a 1mm-step screw thread of 25.88mm in length to connect the cooling channel tightly.

Two permanent ring magnets were placed at the back side of each electrode to form the magnetron with a separating distance of 1cm. The inner magnet was 12.5mm in height and 31.5mm in diameter with a central hole of 17.5mm in diameter, while the outer magnet was 15.2mm in height and 80mm in diameter with a central hole of 40mm in diameter. Therefore, the two magnets were separated by a distance of 10mm around their opposing surfaces. A metallic disk of 69.7mm in diameter and 2.5mm in thickness was used to choke the outer magnet to prevent the magnetic field lines from extending to the backside of the electrode.

The design of dual magnetrons proposed in this work provides two concentric regions of high magnetic field intensity on electrode surface. At these regions, the charged particles are totally confined because the particles escaping from the inner region towards the walls of vacuum chamber will lose some energy and then be trapped by the outer region. In conventional configurations, a fraction of charged particles can escape from the confinement region and hence decrease the ionization rate near the cathode.

The advantage of magnetron on the anode is observed in the film deposition of ferromagnetic materials because the magnetic field intensity forces the deposited particles to distribute on the substrate according to its distribution. This makes possible to produce films with selective optical densities to serve multipurpose devices as in the optical data storage applications [103].

In order to prevent any variation in the arrangement of internal components, a teflon host of 100mm diameter and 44.5mm height with a central groove of 84.75mm diameter and 26.3mm depth was used to maintain the magnetron from the backside of the electrode. This piece was locked from movement by cylindrical teflon piece of 37.5mm in diameter and 35.25mm in height containing an M5 screw driven towards the holder tube.

A single-stage rotary pump (Leybold-Heraeus) of 9 m^3/hr pumping speed was used to get pressure down to about 10^{-3} mbar inside the vacuum chamber. A water-cooled diffusion pump was available for use in this work for lower vacuum pressure and connected to the vacuum chamber via a trap. However, all results presented were obtained using the rotary pump only as vacuum pressure of 10^{-2} mbar was easily reached. The minima of Paschen's curves for the inter-electrode distances 2-6 cm were achieved at pressures higher than 10^{-3} mbar. Pirani gauge (down to 10^{-3} mbar) was used.

The electrical power required for generating discharge inside vacuum chamber was provided by a 5 kV dc power supply (Edwards 2A) through high-tension cables. A current-limiting resistance (3.25 kΩ, 1 kW) was connected between the negative terminal of the dc power supply and the cathode inside the vacuum chamber, while the positive terminal of the dc power supply was connected directly to the anode. The output voltage of the power supply could be varied precisely over 0-5 kV to control the current flowing between discharge electrodes. However, the maximum supply voltage did not exceed 800V. Another dc power supply (0-250 V PHYWE-7532) was used to provide bias potential for Langmuir probe measurements. In addition, a third dc power supply (DHF-1502DD, 1.5-15V, 0.6-2A) was used for electrical measurements performed on the samples prepared as photodetectors.

Gas supply unit consists of argon and nitrogen cylinders, flowmeters, gas flow regulators, needle valves and connections and joints. Argon gas of 96% purity and nitrogen gas of 90% purity were used.

A compact unit was used to cool and circulate the room-temperature water through a channel in discharge electrodes. This unit can cool more than 51 liters of distilled water down to about 4°C and circulate it with maximum flow rate of 30 L/min. The temperature inside the chamber was measured by a thermometer located near the wall of the chamber while the temperatures of both electrodes were measured by thermocouples connected to digital instruments. The maximum surface temperature of the substrate placed on the anode was 40-45°C with uncooled circulating water and reasonably reduced with cooled circulating water.

The operating conditions of the system were classified into two groups; constant and variable. The constant operating conditions include inter-electrode distance, vacuum pressure, current limiting resistance, discharge voltage, discharge current, cooling temperature, cooling water flow rate and deposition time. The variable operating conditions include gas pressure and gas flow rate. Varying discharge voltage was almost possible during the operation. In addition, turning the cooling system off would raise the temperature of either electrode to 40-45°C with circulating water, while stopping the circulation of water would raise electrode temperature more (up to 150°C).

3. Results and Discussion

Electrical characteristics of the discharge plasma were determined by measuring the breakdown voltage and discharge current as functions of inter-electrode distance, gas pressure, gas mixing ratio and supply voltage. High-impedance voltmeters and DC high-precision ammeters were used to perform these measurements.

The electrical characteristics of discharge plasma, such as dependencies of discharge current on the applied voltage and gas pressure inside the vacuum chamber as well as Paschen's curve, are of importance to introduce the homogeneity of the generated plasma. In the following, these characteristics are presented.

In figure (3), the discharge current was measured as a function of discharge voltage at different inter-electrode distances (2-6cm) without magnetron. It is clear that no current flows when the voltage is below 200V as the gas between the electrodes not reached the breakdown. At voltages 200-250, discharge current initiates as the breakdown voltage is reached. Obviously, discharge current flows at smaller distance between the electrodes as the charge carriers (electrons) have to pass shorter distance to transfer from cathode to anode. However, this was not exactly satisfied here due to some experimental imperfections.
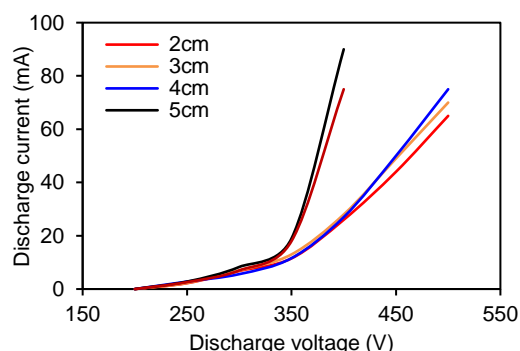

Figure (3) Current-voltage characteristics of argon gas discharge at different inter-electrode distances (2-6cm) and working pressure of 0.7mbar without magnetrons

At certain discharge voltages, the discharge current was measured as a function of inter-electrode distance as shown in figure (4). Initially, this current slightly increases at distance from 2 to 3 cm, slightly decreases at distance of 4 cm, reasonably increases at distance of 5cm, and decreases at distance of 6 cm. This nonlinear behavior between discharge current and discharge voltage is a characteristic of abnormal region in glow discharge.

At certain inter-electrode distance (e.g., 2 cm), the discharge current increases with increasing discharge voltage. This behavior is the same at all distances. At high voltages (>350V), the discharge current is reasonably increased with increasing the distance, while the variation in the discharge current with distance is very small at lower voltages (<300V). The electrodes are fully covered by the discharge and any increase in discharge current leads to an increase in the cathode fall. So, the voltage across the electrodes rises sharply. This behavior is attributed to the mobility-limited version of Child-Langmuir equation, where the discharge current is proportional to $V^{3/2}/d^2$ [110]. As shown in these figures, at inter-electrode distance of 5cm, maximum discharge current was measured.

In case of using a magnetron, the same relation between discharge current and discharge voltage was recorded at certain inter-electrode distance of 4cm, as shown in figure (5). Despite the discharge current measured at this distance was lower than that measured at 5cm, this distance was chosen for this relation to match the optimum distance of magnetron configuration, as shown before.
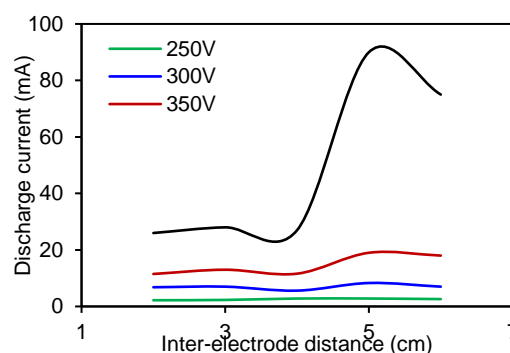

Figure (4) Variation of discharge current with inter-electrode distance at certain discharge voltages without using magnetron

It is clear that higher discharge current is resulted at each discharge voltage compared with the case when using only one magnetron (at the cathode), which in turn shows higher current when compared to no magnetron case. This effect is attributed to the role of magnetron in confining charged particles (electrons and ions) near the electrodes, increasing number of collisions with neutral gas atoms and hence producing much more particles those carry much more charges in time (higher current).

Using only one magnetron at the cathode results in an increase of about 13% in the discharge current compared with the case without magnetron, while using dual magnetrons at both electrodes results in an increase of about 24%.

On the other side, in case of using a magnetron, the variation of discharge current with inter-electrode distance was measured at a discharge voltage of 400V, as shown in figure (6). As in figure (5), similar behaviors were obtained when using only one magnetron (at the cathode) and using dual magnetrons with the values of discharge current shifted upward. Maximum currents were obtained at inter-electrode distance of 5cm.
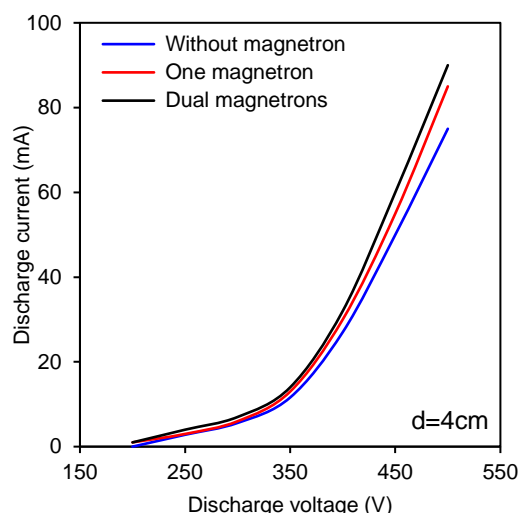

Figure (5) Current-voltage characteristics of discharge plasma at inter-electrode distance of 4cm without magnetron, with only one magnetron and with dual magnetrons

Since one of the main goals of this work is to produce silicon nitride nanostructures, pure nitrogen gas (N_2) is mixed with argon gas (Ar) to form the mixture required for this purpose. Different mixing ratios of $Ar:N_2$ are characterized to determine the optimum ratio at which the required silicon nitride will be prepared, as shown in figure (7).

If nitrogen gas mixed with argon at mixing ratio $Ar:N_2$ of 4:1, an increase in the discharge current was observed, as shown in figure (7), which may be attributed to the contribution to total current from the ionized nitrogen molecules. Ionization of these molecules can occur by collisions with primary electrons under the effect of applied electric field and/or by the secondary electrons. The difference is very small at low discharge voltages (200-300V) because the major contribution of nitrogen molecules is due to the ionization by primary electrons. This difference is clearly observed at high discharge voltages (>300V) because the secondary electrons are accelerated by higher electric field (V/d) and then the ionization of nitrogen molecules by collisions with these electrons is increased.

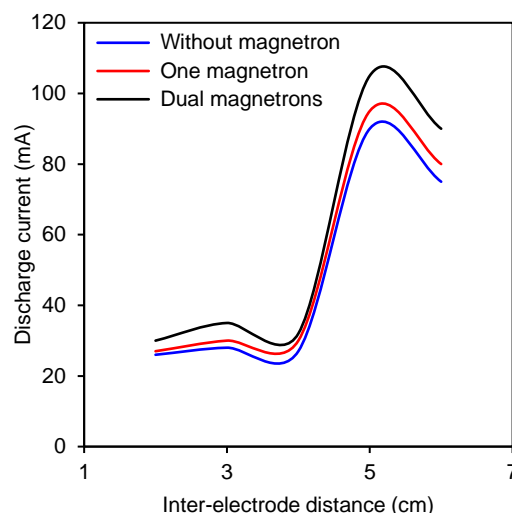Therefore, the contributions of ionized molecules are added.

Figure (6) Variation of discharge current with inter-electrode distance at certain discharge voltage (400V) for the cases without magnetron, using one magnetron and dual magnetrons
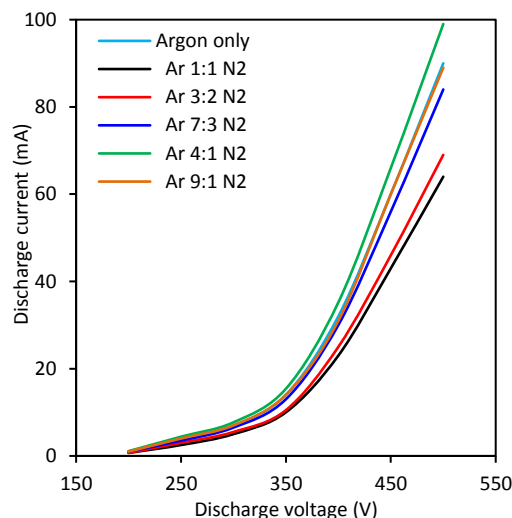

Figure (7) Discharge current-voltage characteristics for different argon/nitrogen mixtures at total gas pressure of 0.7mbar and inter-electrode distance of 4cm

References

[1] F.F. Chen, Introduction to Plasma Physics and Controlled Fusion, 2nd edition, Plenum Press (NY), p. 22 (1974).

[2] T.J. Boyd and J. Sanderson, Physics of Plasmas, Cambridge University Press (2003).

[3] F. Ghaleb and A. Belasri, Numerical and theoretical calculation of breakdown voltage in the electrical discharge, Radiation Effects and Defects in Solids, 1, 1-7 (2012).

[4] M.A. Lieberman and A.J. Lichtenberg, Principles of Plasma Physics and Materials Processing, Second edition, Wiley, p. 547 (2005).

[5] M.M. Mansour, N.M. El-Sayed, O.F. Farag and M.H. Elghazaly, Effect of He and Ar Addition on N_2 Glow Discharge Characteristics and Plasma Diagnostics, Arab J. of Nuclear Sci. and Applications, 46(1), 116-125 (2013).

[6] A.A. Solov'ev, Investigation of Plasma Characteristics in an Unbalanced Magnetron Sputtering System, Plasma Phys. Rep., 35(5), 399–408 (2009).

[7] A. Bojarov, M. Radmilovic-Radjenovic and Z. Petrovic, Effect of the ion induced secondary electron emission on the characteristics of RF plasmas, Publ. Astron. Obs. Belgrade, 89, 131-134 (2010).

[8] T.E. Sheridan, M.J. Goeckner and J. Goree, Model of energetic electron transport in magnetron discharges, J. Vac. Sci. Technol. A, 8(1), 30-37 (1990).

[9] J. Goree and T. E. Sheridan, Magnetic field dependence of sputtering magnetron efficiency, Appl. Phys. Lett., 59(9), 1052-1054 (1991).

[10] J.W. Bradley, Measurements of the sheath potential in low density plasmas, J. Phys. D: Appl. Phys., 25, 1443-1453 (1992).

[11] M.B. Hendricks, Effects of ion-induced electron emission on magnetron plasma instabilities, J. Vac. Sci. Technol. A 12, 1408 (1994)

[12] T.E. Sheridan, M.J. Goeckner and J. Goree, Electron velocity distribution functions in a sputtering magnetron discharge for the ExB direction, J. Vac. Sci. Technol. A 16(4), 2173-2176 (1998).

[13] E. Martines, Electrostatic fluctuations in a direct current magnetron sputtering plasma, Phys. of Plasmas, 8(6), 3042-3050 (2001).

[14] Annemie Bogaerts, Gas discharge plasmas and their applications (Review), Spectrochimica Acta, Part B57, 609–658 (2002).

[15] C.H. Shon and J.K. Lee, Modeling of Magnetron Sputtering Plasmas, Appl. Surf. Sci., 192, 258-269 (2002).

[16] I. Levchenko, Stable plasma configurations in a cylindrical magnetron discharge, Appl. Phys. Lett., 85(12), 2202-2204 (2004).

[17] G. Petraconi, Longitudinal Magnetic Field Effect on the Electrical Breakdown in Low Pressure Gases, Brazilian J. of Physics, 34(4B), 1662-1666 (2004).

[18] M.H. Elghazaly, S. Solyman and A.M. Abdelbaky, Study of Some Basic Transport Coefficients in Noble-Gas Discharge Plasmas, Egypt. J. Solids, 30(1), 137 (2007).

[19] M.A. Hassouba and N. Dawood, Study the Effect of Magnetic Field on the Electrical Characteristics of the Glow Discharge, Adv. in Appl. Sci. Res., 2(4), 123-131 (2011).

[20] Mohammed K. Khalaf, Influence of Discharge Pressure on the Plasma Parameter in a Planar DC-Sputtering Discharge of Argon, Int. J. of Recent Res. Rev., 13-16 (2013).

[21] Sankar M. Borah, Direct Current Magnetron Glow Discharge Plasma Characteristics Study for Controlled Deposition of Titanium Nitride Thin Film, J. of Materials, vol. 2013, article ID 852859.